Nano Research 2015, 8(6): 1944–1955
DOI 10.1007/s12274-015-0704-3
Research Article
ISSN 1998-0124
CN 11-5974/O4

Mass production of Co_3O_4@CeO_2 core@shell nanowires for catalytic CO oxidation

Jiangman Zhen[1,2,§], Xiao Wang[1,§], Dapeng Liu[1] (✉), Zhuo Wang[1,2], Junqi Li[1,2], Fan Wang[1,2], Yinghui Wang[1], and Hongjie Zhang[1] (✉)

[1] *State Key Laboratory of Rare Earth Resource Utilization, Changchun Institute of Applied Chemistry, Chinese Academy of Sciences, Changchun, 130022, Jilin, China*
[2] *University of the Chinese Academy of Sciences, Beijing 100039, China*
[§] *The two authors contribute equally to this work.*

Received: 25 September 2014
Revised: 03 December 2014
Accepted: 23 December 2014

KEYWORDS
Co_3O_4@CeO_2,
core@shell,
nanowires,
CO oxidation,
synergistic effects

ABSTRACT

In this study, Co_3O_4@CeO_2 core@shell nanowires were successfully prepared via thermal decomposition of $Co(CO_3)_{0.5}(OH)\cdot 0.11H_2O$@$CeO_2$ core@shell nanowire precursors. As a CO oxidation catalyst, Co_3O_4@CeO_2 shows remarkably enhanced catalytic performance compared to Co_3O_4 nanowires and CeO_2 nanoparticles (NPs), indicating obvious synergistic effects between the two components. It also suggests that the CeO_2 shell coating can effectively prevent Co_3O_4 nanowires from agglomerating, hence effecting a substantial improvement in the structural stability of the Co_3O_4 catalyst. Furthermore, the fabrication of the well-dispersed core@shell structure results in a maximized interface area between Co_3O_4 and CeO_2, as well as a reduced Co_3O_4 size, which may be responsible for the enhanced catalytic activity of Co_3O_4@CeO_2. Further examination revealed that CO oxidation may occur at the interface of Co_3O_4 and CeO_2. The influence of calcination temperatures and the component ratio between Co_3O_4 and CeO_2 were then investigated in detail to determine the catalytic performance of Co_3O_4@CeO_2 core@shell nanowires, the best of which was obtained by calcination at 250 °C for 3 h with a Ce molar concentration of about 38.5%. This sample achieved 100% CO conversion at a reduced temperature of 160 °C. More importantly, more than 2.5 g of the Co_3O_4@CeO_2 core@shell nanowires were produced in one pot by this simple process, which may be beneficial for practical applications as automobile-exhaust gas-treatment catalysts.

1 Introduction

Catalytic oxidation of carbon monoxide (CO) has drawn considerable attention because of the serious health effects associated with exposure to CO. Co_3O_4, a typical spinel-structure transition metal oxide, has

Address correspondence to Dapeng Liu, liudp@ciac.ac.cn; Hongjie Zhang, hongjie@ciac.ac.cn

garnered intense interest recently because of its excellent catalytic CO oxidation capability, and is regarded as an alternative to noble metal catalysts [1–5]. Co_3O_4 nanorods synthesized by Xie's group exhibited good catalytic performance, catalyzing CO oxidation at a low temperature of −77 °C in a trace moist stream of normal feed gas [2]. They attributed this to the abundance of active Co^{3+} species on the {110} planes of the Co_3O_4 nanorods. Additionally, the size of the Co_3O_4 nanostructure is also thought to affect its catalytic activity [4, 5]. However, there are few reports on optimizing the stability of Co_3O_4 catalysts, because, for practical needs, catalysts are often required to work at relatively high temperatures without removing a mass of streams. Under such conditions, nanomaterials are liable to aggregate or deform, resulting in a substantial loss of catalytic active centers and serious catalytic deterioration or even inactivation. Therefore, the synthesis of Co_3O_4 catalysts with high activity and stability has become an area of great focus in material science.

Fabrication of core@shell structures has been identified as an efficient way to inhibit agglomeration so as to improve the stability of nanomaterials [6–15]. In this regard, numerous types of oxides, such as CeO_2, SiO_2, and ZrO_2, have been adopted as stable shell components [6–8, 12, 15]. In particular, CeO_2, a typical multifunctional rare earth oxide, has received intense scrutiny owing to its wide applications in catalysis [16–25]. It has a high oxygen-storage capacity, making it highly active in oxidation reactions. More importantly, it can also exhibit excellent synergistic effects with other active catalytic components. For instance, Ag@CeO_2, Pt@CeO_2, Au@CeO_2, and Pd@CeO_2 core@shell catalysts exhibit good activity and high-temperature stability as oxidation reaction catalysts [12, 22–25]. Hence, it is considered likely that both the activity and stability of Co_3O_4 catalyst could be optimized through the facile fabrication of Co_3O_4@CeO_2 core@shell structures.

Generally, core@shell structures are synthesized through the hydrolysis of precursors to deposit the shell component onto a preformed core [25]. However, it is necessary to perform surface modification on the core in advance, in order to avoid independent nucleation of the shell component. This layer-by-layer technology is a multistep process that requires precise control and complex surface modification, which is not conducive to large-scale synthesis and has seriously limited the practical applications of such catalysts. Alternatively, the reverse-micelle method can be used to prepare core@shell structures [6, 9]. However, this synthetic procedure is also a multistep method and requires considerable time and energy. Meanwhile, to produce specific core@shell structures, organic species such as surfactants have been used typically [25, 26]; some of these are difficult to remove completely, and hence the catalytic active centers of nanocatalysts can become contaminated, resulting in unsatisfactory catalytic activity. Consequently, it is a critical goal to develop an effective means for the facile, clean mass production of Co_3O_4@CeO_2 core@shell structures.

Here, we report the synthesis of high-quality Co_3O_4@CeO_2 core@shell structures in gram-scale quantities. First, $Co(CO_3)_{0.5}(OH)\cdot 0.11H_2O$ nanowires were prepared as precursors [27]. They were then coated by a CeO_2 shell, and subjected to a previously reported strategy [28]. After calcination in air, the as-obtained $Co(CO_3)_{0.5}(OH)\cdot 0.11H_2O$@$CeO_2$ core@shell nanowires were thermally decomposed and transformed into the final monodisperse Co_3O_4@CeO_2 core@shell nanowires consisting of Co_3O_4 and CeO_2 nanoparticles (NPs). In order to investigate the transformation process, thermal gravimetric analysis (TGA) of $Co(CO_3)_{0.5}(OH)\cdot 0.11H_2O$@$CeO_2$ was performed in conjunction with CO catalytic testing and X-ray diffraction (XRD), scanning electron microscope (SEM), and transmission electron microscopic (TEM) analyses. Then, the influence of calcination temperatures and the component ratio between Co_3O_4 and CeO_2 on the catalytic performance of Co_3O_4@CeO_2 core@shell nanowires were systematically investigated to determine the optimal conditions for catalytic CO oxidation.

2 Experimental

Preparation of $Co(CO_3)_{0.5}(OH)\cdot 0.11H_2O$ nanowires (Co precursor): $Co(CO_3)_{0.5}(OH)\cdot 0.11H_2O$ nanowires were synthesized by a previously reported hydrothermal procedure [27]. Here, 0.56 g of $CoSO_4\cdot 7H_2O$ was dissolved in 40 mL of a mixture containing 7 mL of glycerol and 33 mL of deionized water. After being stirred for about 10 min, a transparent solution was

obtained, into which 0.10 g of urea was added. Thirty minutes later, the solution was transferred into a 50 mL Teflon-lined stainless steel autoclave, followed by heating at 170 ℃ for a period of 24 h in an electric oven. Afterwards the autoclave was cooled passively to room temperature. The products were collected and washed with deionized water and ethanol three times by centrifugation; they were then dried at 60 ℃ overnight.

***Preparation of $Co(CO_3)_{0.5}(OH)\cdot 0.11H_2O@CeO_2$ core@shell nanowires (Co precursor@CeO_2)*:** 0.1 g of $Co(CO_3)_{0.5}(OH)\cdot 0.11H_2O$ nanowires were ultrasonically dispersed in a mixed solution of 50 mL water and 50 mL ethanol. Then, 0.65 mmol $Ce(NO_3)_3$ and 20 mL of 0.02 g/mL hexamethylenetetramine (HMT) aqueous solution were added in turn. The temperature of the solution was then increased to 70 ℃ and refluxed for 2 h before being cooled to room temperature. The products were purified by centrifugation and washed with deionized water and ethanol three times, and then dried at 60 ℃. This product was named $Co(CO_3)_{0.5}(OH)\cdot 0.11H_2O@CeO_2$-1. By tuning the amount of $Ce(NO_3)_3$ and HMT, another three $Co(CO_3)_{0.5}(OH)\cdot 0.11H_2O@CeO_2$ precursors were synthesized by the above procedure. The as-obtained products were named $Co(CO_3)_{0.5}(OH)\cdot 0.11H_2O@CeO_2$-2 (1.3 mmol $Ce(NO_3)_3$, 30 mL HMT solution), $Co(CO_3)_{0.5}(OH)\cdot 0.11H_2O@CeO_2$-3 (0.325 mmol $Ce(NO_3)_3$, 10 mL HMT solution), and $Co(CO_3)_{0.5}(OH)\cdot 0.11H_2O@CeO_2$-4 (0.16 mmol $Ce(NO_3)_3$, 5 mL HMT solution).

***Preparation of $Co_3O_4@CeO_2$ core@shell nanowires*:** The precursors of $Co(CO_3)_{0.5}(OH)\cdot 0.11H_2O@CeO_2$-1 were calcined at 250, 350, and 500 ℃ for 3 h in air, and the corresponding products were named $Co_3O_4@CeO_2$-1-250, $Co_3O_4@CeO_2$-1-350 and $Co_3O_4@CeO_2$-1-500. For a control, $Co(CO_3)_{0.5}(OH)\cdot 0.11H_2O@CeO_2$-2, -3, and -4 were all calcined at 250 ℃ for 3 h in air as well, and the corresponding products were named $Co_3O_4@CeO_2$-2-250, $Co_3O_4@CeO_2$-3-250, and $Co_3O_4@CeO_2$-4-250.

***Preparation of Co_3O_4 nanowires*:** $Co(CO_3)_{0.5}(OH)\cdot 0.11H_2O$ nanowires were directly calcined at 250 ℃ for 3 h in air.

***Preparation of Co_3O_4-CeO_2 hybrids*:** 0.03 g of the as-prepared Co_3O_4 nanowires were ultrasonically dispersed in a mixed solution of 12 mL water and 12 mL ethanol, and then 0.24 mmol $Ce(NO_3)_3$ and 10 mL of 0.02 g/mL HMT aqueous solution were added in turn. Then, the temperature of the solution was increased to 70 ℃ and refluxed for 2 h before being cooled to room temperature. The products were purified by centrifugation and washed with deionized water and ethanol three times, and then dried at 60 ℃.

***Preparation of pure CeO_2 NPs*:** 1 mmol $Ce(NO_3)_3$ was dissolved in a mixed solution of 20 mL deionized water and 20 mL ethanol. Then, 25 mL of 0.02 g/mL HMT aqueous solution was added. The temperature of the mixture was then increased to 70 ℃ and refluxed for 2 h before being cooled to room temperature. The products were purified by centrifugation and washed with deionized water and ethanol three times, and then dried at 60 ℃. Finally, the products were calcined in air at 250 ℃ for 3 h in air.

***Preparation of Co_3O_4–CeO_2 mixtures*:** 0.058 g of the above-mentioned Co_3O_4 nanowires and 0.042 g of CeO_2 NPs were physical mixed by grinding in an agate mortar for 30 min.

***Characterization*:** XRD data were collected on a Rigaku-*D*/max 2,500 V X-ray diffractometer with Cu-K_α radiation (λ = 1.5418 Å), with an operation voltage and current maintained at 40 kV and 40 mA. TEM images were obtained with a TECNAI G2 high-resolution transmission electron microscope (HRTEM) operating at 200 kV. A HITACHI S-4800 field-emission scanning electron microscope (FE-SEM) was used to characterize the morphology of the samples. X-ray photoelectron spectroscopy (XPS) was performed on an ESCALAB-MKII 250 photoelectron spectrometer (VG Co.) with Al-K_α X-ray radiation as the X-ray excitation source. TGA curves of the samples were acquired by using a SDT 2960 thermal analyzer at a heating rate of 10 ℃·min^{-1} in air atmosphere within a temperature range of 20 to 700 ℃. A GC 9800 gas chromatography tester was employed to obtain the samples' CO-conversion curves. N_2 sorption isotherms were obtained at 77 K on an Auto-sorb-1 apparatus. Inductively coupled plasma (ICP) analyses were performed with a Varian Liberty 200 spectrophotometer to determine Ce content. H_2-temperature-programmed

reduction (TPR) was conducted on a TPDRO 1100 apparatus supplied by the Thermo-Finnigan Company. Before detection by the TCD, the gas was purified by a trap containing CaO + NaOH materials in order to remove the H_2O and CO_2. For each iteration, 30 mg of a sample was heated from room temperature to 900 ℃ at a rate of 10 ℃/min. A gaseous mixture of 5 vol.% H_2 in N_2 was used as reductant at a flow rate of 20 mL/min.

***Catalytic tests*:** 25 mg of catalyst was placed in a stainless-steel reaction tube. The CO oxidation catalytic tests were performed under an atmosphere of 1% CO and 20% O_2 in N_2 at a fixed space velocity of 50 mL/min. The composition of the gas was monitored online by gas chromatography.

3 Results and discussion

The as-obtained samples were characterized by SEM and TEM. From the SEM and TEM images (Figs. 1(a) to 1(c)), it can be clearly seen that Co precursor is composed by uniform and well-dispersed nanowires of several micrometers in length and tens of nanometers in width. After being coated with a CeO_2 shell, the smooth surface of each Co precursor nanowire is noticeably roughened (Figs. 1(d) to 1(f)), indicating a successful CeO_2 shell-coating process. The as-prepared products maintained the wire-like morphology as the Co precursor and each nanowire were completely wrapped by a shell composed of hundreds of self-assembled 6 nm CeO_2 NPs. The inset in Fig. 1(f) indicates a lattice spacing of 0.31 nm, which corresponds to the characteristic (111) plane of fluorite-phase CeO_2. Combining this with the XRD results (Fig. S1 in the Electronic Supplementary Material (ESM)), we have strong evidence for the core@shell-structure formation of $Co(CO_3)_{0.5}(OH)\cdot 0.11H_2O@CeO_2$. More than 3 g of $Co(CO_3)_{0.5}(OH)\cdot 0.11H_2O@CeO_2$ can be obtained in one pot (see Fig. S2 in the ESM), and its schematic fabrication is summarized as a two-step process in Scheme 1.

Catalytic oxidation of CO is chosen here as the model reaction for evaluating the catalytic performance of the samples. In order to study the details of the transformation of $Co(CO_3)_{0.5}(OH)\cdot 0.11H_2O$ as well as its influence on catalytic performance, CO oxidation cycling tests of $Co(CO_3)_{0.5}(OH)\cdot 0.11H_2O@CeO_2$-1 were performed in temperatures ranging from 50 to 250 ℃. As shown in Figs. 2 and S3 in the ESM, it can be observed that, during the tests, the value of T_{100} (the temperature for 100% CO conversion) decreased until the fifth cycle (to 160 ℃) and then remained stable at 160 ℃ in the following cycles. In general, catalysts

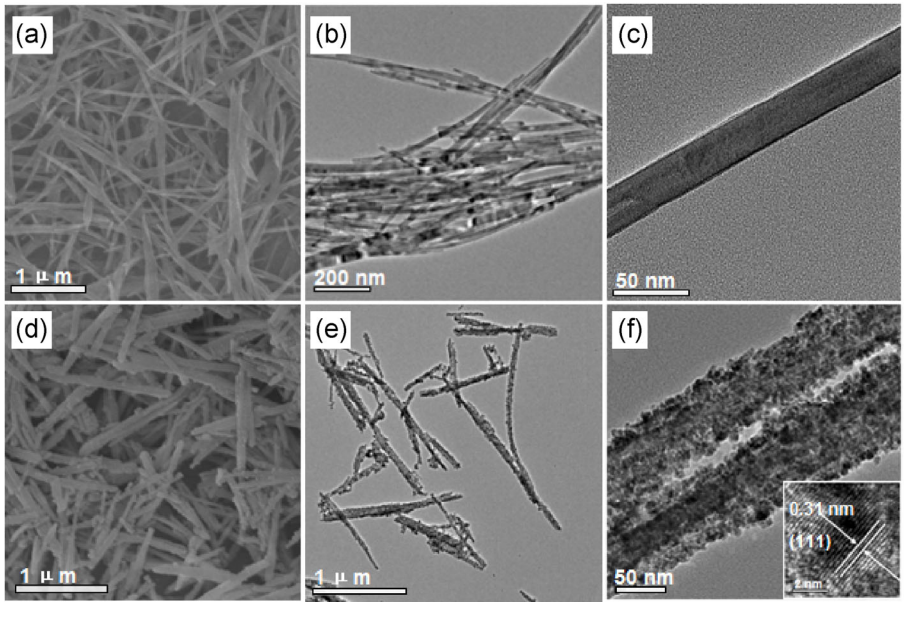

Figure 1 (a) SEM and ((b) and (c)) TEM images of Co precursor; (d) SEM and ((e) and (f)) TEM images of Co precursor@CeO_2 (Inset: HRTEM of CeO_2).

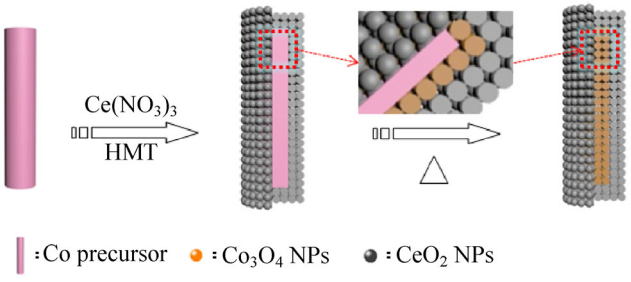

Scheme 1 Schematic for the preparation process of Co_3O_4@CeO_2 core@shell nanowires.

often degrade more or less under long-term and high-temperature catalytic conditions due to aggregation, growth, or other such as contamination. This abnormal enhancement of catalytic activity prompted us to investigate this phenomenon in depth.

As reported by Lou et al. [27], the transformation of $Co(CO_3)_{0.5}(OH)\cdot 0.11H_2O$ to Co_3O_4 starts at about 200 ℃; thus, it is presumed that such transformation would proceed during the catalytic process. Firstly, TGA was employed to obtain detailed information regarding the decomposition process of $Co(CO_3)_{0.5}(OH)\cdot 0.11H_2O$@$CeO_2$-1. Figure 3 shows that the major weight loss (about 10%) takes place in the temperature range of 230 to 300 ℃, which is consistent with the corresponding DSC analysis (Fig. S4 in the ESM). This portion of the loss can be attributed to the decomposition of carbonates and hydroxide groups of $Co(CO_3)_{0.5}(OH)\cdot 0.11H_2O$ [27]. Coincidentally, the first cycling curve of CO conversion fully supports the TGA–DSC results that, above 230 ℃, the sample can totally catalyze CO oxidation due to the transformation of $Co(CO_3)_{0.5}(OH)\cdot 0.11H_2O$ into Co_3O_4.

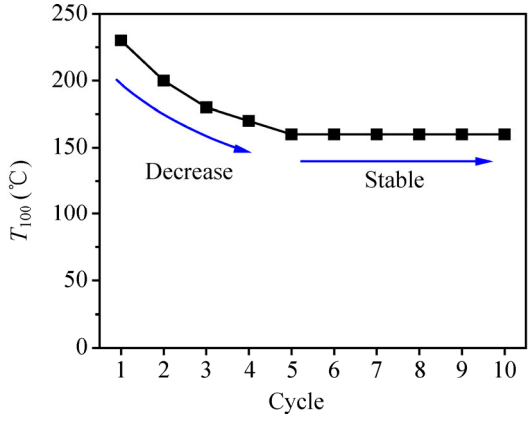

Figure 2 Cycling tests of $Co(CO_3)_{0.5}(OH)\cdot 0.11H_2O$@$CeO_2$-1 for CO conversion.

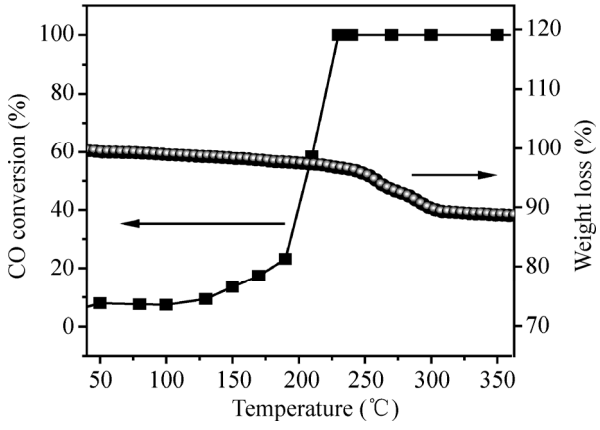

Figure 3 TGA curve and the first cycling curve of CO conversion of $Co(CO_3)_{0.5}(OH)\cdot 0.11H_2O$@$CeO_2$-1.

Further insight into the transformation of $Co(CO_3)_{0.5}(OH)\cdot 0.11H_2O$@$CeO_2$-1 requires XRD analysis. After ten cycling tests for CO oxidation, a sample was collected and labeled "$Co(CO_3)_{0.5}(OH)\cdot 0.11H_2O$@$CeO_2$-1-after 10". In Fig. 4, it can be clearly seen that the heat treatment during the cycling tests results in obvious transformation of orthorhombic-phase $Co(CO_3)_{0.5}(OH)\cdot 0.11H_2O$ into spinel-phase Co_3O_4—that is, the intensity of the corresponding peak of $Co(CO_3)_{0.5}(OH)\cdot 0.11H_2O$ decreased quickly, but that of Co_3O_4 was gradually enhanced. Based on the above analysis of CO catalysis associated with TGA and XRD curves, it can be concluded that the transformation of $Co(CO_3)_{0.5}(OH)\cdot 0.11H_2O$ into Co_3O_4 occurred throughout the cycling-test process; this may stem from the surface regions of the $Co(CO_3)_{0.5}(OH)\cdot 0.11H_2O$ nanowires and move toward their interior. As the cycling tests continued, more and more $Co(CO_3)_{0.5}(OH)\cdot 0.11H_2O$ was decomposed; and, after five cycles, its surface regions that performed catalytic CO oxidation transformed completely into Co_3O_4. This explains why, at this stage, their catalytic activity improved and that T_{100} decreased continuously. For the last five cycles, the conversion may have proceeded within the interior regions of the $Co(CO_3)_{0.5}(OH)\cdot 0.11H_2O$ nanowires. Therefore, the T_{100} became constant. These results suggest that only the surface Co_3O_4 components adjacent to CeO_2 worked well for catalytic CO oxidation. In other words, CO oxidation might takes place at the interface of the Co_3O_4 and CeO_2 components [29, 30].

To confirm this notion on the catalytic CO oxidation process, we kept a constant calcination temperature of 250 ℃ and prolonged the calcination time to 3 h to effect a complete transformation of $Co(CO_3)_{0.5}(OH)\cdot 0.11H_2O$ into Co_3O_4. The as-obtained product is labeled as Co_3O_4@CeO_2-1-250. Its corresponding XRD pattern (Fig. 4) shows that the peaks of $Co(CO_3)_{0.5}(OH)\cdot 0.11H_2O$ disappear completely, while the peak intensity of Co_3O_4 becomes more intense. TEM (Fig. 5) and SEM images (Fig. S5 in the ESM) show that the wire-like structure was preserved after either CO catalytic testing or calcination. Elemental mapping indicated that elemental Co was only present in the cores of the nanowires, while elemental Ce was more widely distributed, which is a typical shell feature. The absence of Co peaks and the presence of Ce peaks in the XPS spectrum of Co_3O_4@CeO_2-1-250 (see Fig. S6 in the ESM) further verify the thick shell coating of CeO_2. The catalytic test shows that Co_3O_4@CeO_2-1-250 can also catalyze 100% CO conversion at 160 ℃ (see Fig. 6), which is the same with that of $Co(CO_3)_{0.5}(OH)\cdot 0.11H_2O$@$CeO_2$-1-after 10. All these observations point to the fact that $Co(CO_3)_{0.5}(OH)\cdot 0.11H_2O$@$CeO_2$ should pass through an intermediate core@shell@shell state of $Co(CO_3)_{0.5}(OH)\cdot 0.11H_2O$@$Co_3O_4$@$CeO_2$ before finally forming Co_3O_4@CeO_2, as described in Scheme 1. Despite the differences in the core components of $Co(CO_3)_{0.5}(OH)\cdot 0.11H_2O$@$Co_3O_4$-1-after 10 and Co_3O_4@CeO_2-1-250, they exhibit similar catalytic activities. This strongly indicates that only the surface Co_3O_4 components that interfaced with CeO_2 performed well in terms of catalytic CO oxidation.

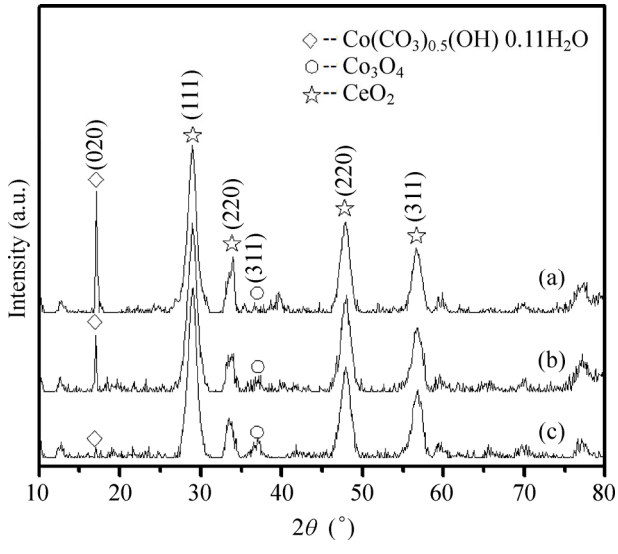

Figure 4 XRD spectra of (a) $Co(CO_3)_{0.5}(OH)\cdot 0.11H_2O$@$CeO_2$-1, (b) $Co(CO_3)_{0.5}(OH)\cdot 0.11H_2O$@$CeO_2$-1-after 10, and (c) Co_3O_4@CeO_2-1-250.

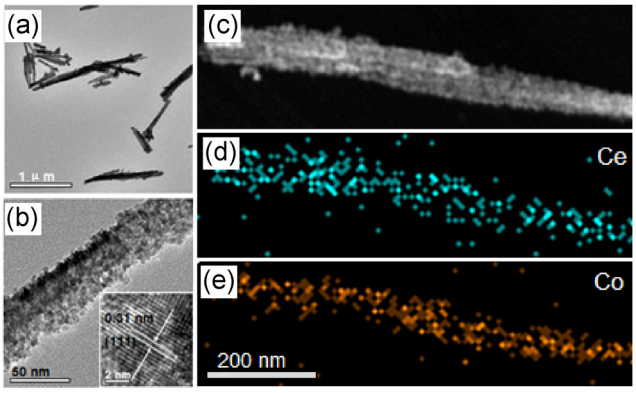

Figure 5 ((a) to (c)) TEM images of Co_3O_4@CeO_2-1-250 and ((d) and (e)) corresponding EDX-mapping analysis.

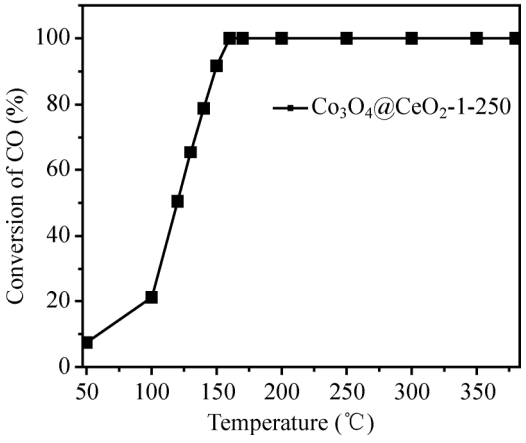

Figure 6 CO conversion curve for Co_3O_4@CeO_2-1-250.

However, until now it remained uncertain whether coating with a CeO_2 shell could improve catalytic activity and stability against calcination of Co_3O_4 nanowires. Thus, comparative studies have been performed with the following four substances: Co_3O_4 nanowires, Co_3O_4–CeO_2 mixtures, Co_3O_4–CeO_2 hybrids, and pure CeO_2 NPs (see Section 2). As shown in Figs. 7 and S7 in the ESM, all of the as-obtained Co_3O_4 nanowire samples lost their original wire-like morphology, and most of them aggregated into bundles. In contrast, Co_3O_4@CeO_2-1-250 exhibited a well-dispersed, wire-like core@shell structure. This reveals that the CeO_2 shell coating effectively prevented these nanowires from aggregation when calcined.

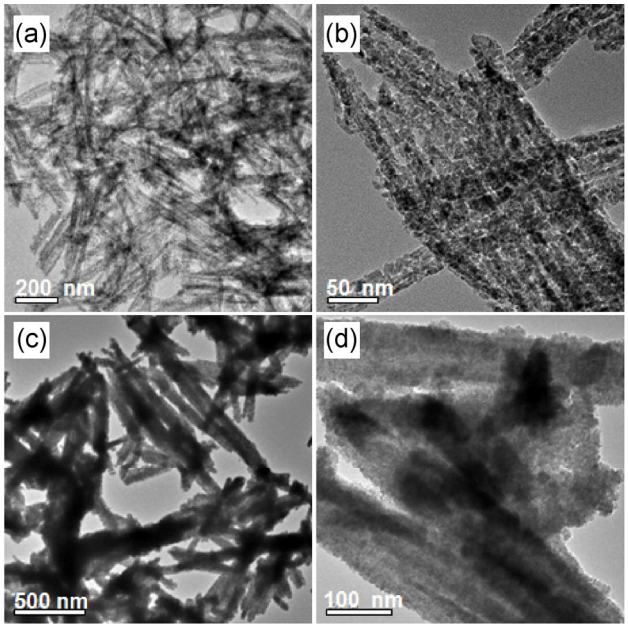

Figure 7 ((a) and (b)) TEM images of Co_3O_4 nanowires, and ((c) and (d)) Co_3O_4–CeO_2 hybrids.

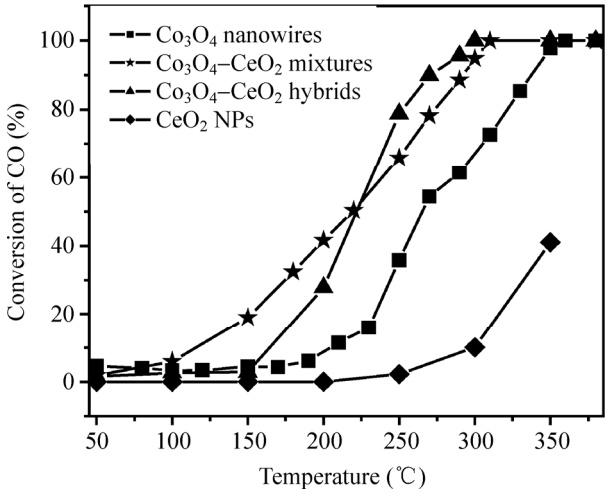

Figure 8 CO conversion curves of Co_3O_4 nanowires, Co_3O_4–CeO_2 mixtures, Co_3O_4–CeO_2 hybrids, and pure CeO_2 NPs.

For Co_3O_4–CeO_2 hybrids, the CeO_2 shell coating was fabricated after the calcination process, resulting in irregular CeO_2 coated Co_3O_4 bundles. In other words, the CeO_2 shell coating should be applied before calcination to prevent the Co_3O_4 nanowires from aggregating, which results in a remarkably improved structural stability of Co_3O_4 catalysts. The sizes of Co_3O_4 NPs in Co_3O_4 nanowires, Co_3O_4–CeO_2 mixtures, and Co_3O_4–CeO_2 hybrids are 9.9, 10.0, and 10.1 nm, respectively (XRD patterns, see Fig. S8 in the ESM), calculated by the Scherrer equation. However, the Co_3O_4 NPs in Co_3O_4@CeO_2-1-250 are much smaller (about 5.9 nm). Obviously, the coating of CeO_2 shell leads to much smaller Co_3O_4 NPs, which might be responsible for the optimization of catalytic activity.

Next, we discuss the influence of the CeO_2 shell on the catalytic activity of Co_3O_4 catalysts. As shown in Fig. 8, Co_3O_4 nanowires can catalyze 100% CO conversion at 360 ℃. Meanwhile, the CO conversion for pure CeO_2 NPs was only 40% at 350 ℃. Although Co_3O_4–CeO_2 mixtures and Co_3O_4–CeO_2 hybrids can catalyze 100% CO conversion at lower temperatures of about 320 and 300 ℃, respectively, the enhancement of their catalytic activity could be ascribed to the synergistic effects between Co_3O_4 and CeO_2 [29–31]. However, Co_3O_4@CeO_2-1-250 can catalyze 100% CO conversion at a much lower temperature of 160 ℃. The optimal catalytic activity of Co_3O_4@CeO_2-1-250 compared to Co_3O_4–CeO_2 mixtures and Co_3O_4–CeO_2 hybrids could be ascribed to the fabrication of the well-dispersed core@shell structures in terms of the following characteristics: (1) The maximized interface area resulting from the well-dispersed core@shell structure, which is beneficial for CO oxidation; (2) the smaller Co_3O_4 size resulting from the effective CeO_2 shell coating of the core@shell structure. This comparative test supports the above hypothesis that the fabrication of Co_3O_4@CeO_2 core@shell structures is efficient for optimizing the catalytic activity and stability of Co_3O_4 catalysts.

It is well known that calcination process has a fundamental impact on the physical and chemical properties of materials [3, 32]. Calcination time, calcination atmosphere, and especially calcination temperature, can greatly affect the catalytic performance of catalysts [12, 26]. Thus, the effects of calcination temperature needed to be further investigated with regard to our core@shell catalysts. As such, $Co(CO_3)_{0.5}(OH)\cdot 0.11H_2O$@$CeO_2$-1 precursors were calcined at 350 and 500 ℃, and these products were named Co_3O_4@CeO_2-1-350 and Co_3O_4@CeO_2-1-500, respectively. As shown in Figs. S9 and S10 in the ESM, Co_3O_4@CeO_2-1-350 and Co_3O_4@CeO_2-1-500 have wire-like core@shell structures comparable with Co_3O_4@CeO_2-1-250.

The XRD patterns in Fig. 9 show that the peaks of CeO_2 show no difference between Co_3O_4@CeO_2-1-250, Co_3O_4@CeO_2-1-350, and Co_3O_4@CeO_2-1-500. However, there are some obvious differences in the Co_3O_4 peaks among the three samples. As the calcination temperature was increased from 250 ℃ to 350 ℃ and then to 500 ℃, the intensity of the Co_3O_4 peaks became stronger and sharper, indicating a better crystallinity of Co_3O_4@CeO_2-1-500 than Co_3O_4@CeO_2-1-350 and Co_3O_4@CeO_2-1-250. The sizes of the Co_3O_4 NPs were 5.9, 10.1, and 12.7 nm for Co_3O_4@CeO_2-1-250, Co_3O_4@CeO_2-1-350, and Co_3O_4@CeO_2-1-500, respectively. The XPS spectra of Co_3O_4@CeO_2-1-350 and Co_3O_4@CeO_2-1-500 in Fig. S11 in the ESM both show five Ce peaks and no obvious Co peaks, which is similar to Co_3O_4@CeO_2-1-250. This suggests that both Co_3O_4@CeO_2-1-350 and Co_3O_4@CeO_2-1-500 have a CeO_2 shell coating comparable to Co_3O_4@CeO_2-1-250. The N_2 adsorption–desorption isotherm of the three samples is shown in Fig. S12 in the ESM, indicating a Type IV behavior of nanoporous Co_3O_4@CeO_2-1-250, Co_3O_4@CeO_2-1-350, and Co_3O_4@CeO_2-1-500 with high surface areas of 144.9, 121.4, and 64.0 $m^2 \cdot g^{-1}$ and average pore widths of 6.14, 8.11, and 9.79 nm, respectively.

Catalytic CO oxidation testing (Fig. 10) was then conducted to evaluate the catalytic performance of Co_3O_4@CeO_2-1-350 and Co_3O_4@CeO_2-1-500 compared with Co_3O_4@CeO_2-250. The T_{100} of the three Co_3O_4@CeO_2 samples follows the order: Co_3O_4@CeO_2-1-250 (160 ℃) < Co_3O_4@CeO_2-1-350 (250 ℃) < Co_3O_4@CeO_2-1-500 (>380 ℃). Co_3O_4@CeO_2-1-250, which is obtained by calcination at the lowest temperature, shows the highest catalytic activity. Next, in order to study the synergetic effects of Co_3O_4 and CeO_2, the catalysts were investigated by H_2-TPR. The two broad TPR peaks (Fig. 11(a)) observed at 380 ℃ and 750 ℃ for CeO_2 can be attributed to the reduction of surface-capping oxygen and bulk oxygen of CeO_2, respectively [12, 33]. The two peaks at around 374 ℃ and 487 ℃ in Fig. 11(b) can be attributed to the two reduction steps of the Co_3O_4 species [1]. It can be seen from Figure 11c–11e that the Co_3O_4 reduction peaks of Co_3O_4@CeO_2-1-250, Co_3O_4@CeO_2-1-350, and Co_3O_4@CeO_2-1-500 all

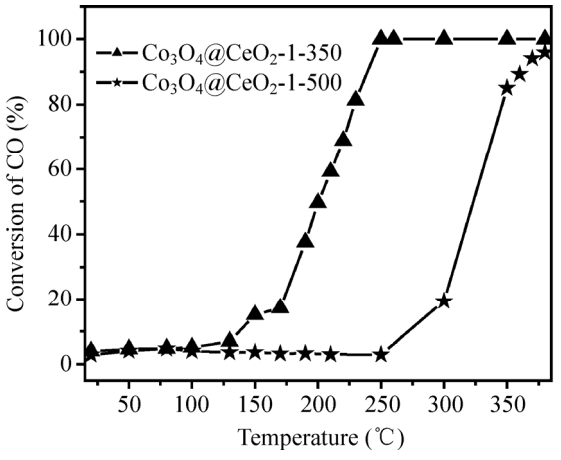

Figure 10 CO conversion curves of Co_3O_4@CeO_2-1-350 and Co_3O_4@CeO_2-1-500.

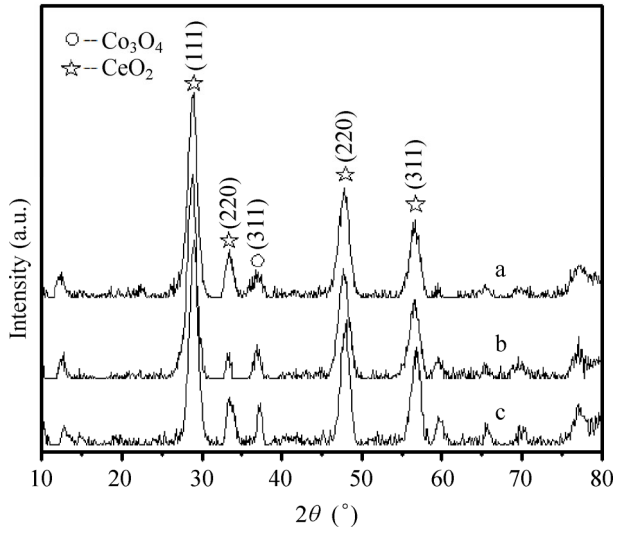

Figure 9 XRD patterns of (a) Co_3O_4@CeO_2-1-250, (b) Co_3O_4@CeO_2- 1-350, and (C) Co_3O_4@CeO_2-1-500.

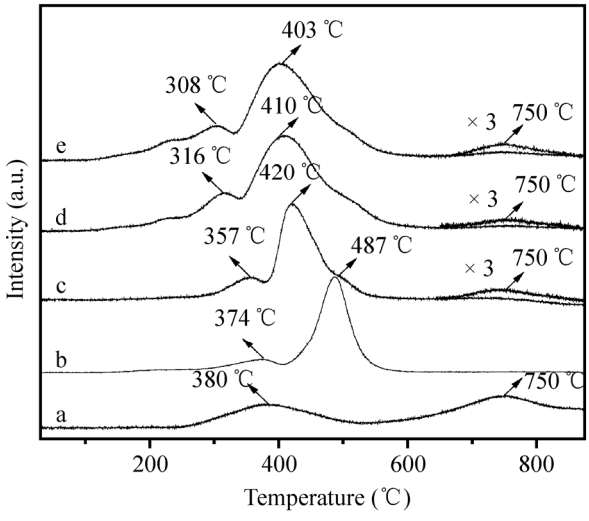

Figure 11 H_2-TPR profiles: (a) pure CeO_2; (b) Co_3O_4 nanowires; (c) Co_3O_4@CeO_2-1-500; (d) Co_3O_4@CeO_2-1-350; and (e) Co_3O_4@CeO_2-1-250.

shifted towards lower temperatures of about 308, 316, and 357 ℃ for the first peak and 403, 410, and 420 ℃ for the second peak, respectively, indicating a typical synergistic effect between Co_3O_4 and CeO_2. A previous work reported that a lower calcination temperature favors reducing the degree of Co_3O_4@CeO_2 interface breakage, which improves the oxidizability of Co_3O_4 [26]. This explains why the oxidizability of Co_3O_4 in these samples follows the sequence: Co_3O_4@CeO_2-1-250 > Co_3O_4@CeO_2-1-350 > Co_3O_4@CeO_2-1-500, which is in agreement with the changing trends of their catalytic activities. If we enlarge the curve in the temperature range of 650 ℃ to 900 ℃ for three iterations, the signal at 750 ℃ for CeO_2 was still clearly seen, indicating the presence of bulk oxygen in CeO_2. Based on the above results and discussions, it can be concluded that the optimal catalytic activity of Co_3O_4@CeO_2-1-250 can be summarized as follows: (1) improved oxidizability of Co_3O_4, which might be caused by the lower degree of Co_3O_4@CeO_2 interface breakage, resulting from the lower calcination temperature [26]; (2) the smaller-sized Co_3O_4 NPs compared with the other two samples; (3) the larger BET surface area than the other two samples [34]; (4) poor crystallinity of Co_3O_4@CeO_2-1-250 that may impart more surface defects and thus higher surface energy, which would favor CO adsorption, resulting in optimal catalytic activity for CO oxidation [3].

Besides calcination temperatures, the component ratio of hetero-catalysts also plays a significant role in catalytic performance [33]. Thus, by simply varying the amount of $Ce(NO_3)_3$, a series of Co_3O_4@CeO_2 core@shell nanowires were synthesized to investigate the effects of the component ratio between Co_3O_4 and CeO_2 on catalytic activity. The corresponding samples are named Co_3O_4@CeO_2-2-250, Co_3O_4@CeO_2-3-250, and Co_3O_4@CeO_2-4-250 (for experimental details see Section 2). As shown in Figs. S13 and S14 in the ESM, the three comparative samples have core@shell wire-like structures comparable to Co_3O_4@CeO_2-1-250, except for the CeO_2 shell thickness. The average diameters of Co_3O_4@CeO_2 core@shell nanowires, estimated by the size distribution data, are 120, 95, 65, and 53 nm for Co_3O_4@CeO_2-2-250, Co_3O_4@CeO_2-1-250, Co_3O_4@CeO_2-3-250, and Co_3O_4@CeO_2-4-250 respectively, indicating that the corresponding average CeO_2 shell thicknesses becomes progressively thinner. The Co and Ce content were determined by ICP-MS. As shown in Table S1 in the ESM, the Ce molar content values are 50.3%, 38.5%, 18.2%, and 8.9% for Co_3O_4@CeO_2-2-250, Co_3O_4@CeO_2-1-250, Co_3O_4@CeO_2-3-250, and Co_3O_4@CeO_2-4-250, respectively. Figure S15 in the ESM presents XRD patterns for Co_3O_4@CeO_2-2-250, Co_3O_4@CeO_2-3-250, and Co_3O_4@CeO_2-4-250. Here, the peak positions and shapes of the three samples are comparable to Co_3O_4@CeO_2-1-250, whereas the intensity ratio of the CeO_2 to Co_3O_4 peaks decreased with decreasing CeO_2 shell thickness.

The catalytic performance for CO oxidation of the three comparative samples was evaluated; the results are shown in Fig. 12. The catalytic activity of the samples is ordered as follows: Co_3O_4@CeO_2-1-250 (160 ℃) > Co_3O_4@CeO_2-3-250 (170 ℃) > Co_3O_4@CeO_2-2-250 (240 ℃) > Co_3O_4@CeO_2-4-250 (270 ℃). Figure 13 presents the relationship between T_{100} and the Ce molar content of the Co_3O_4@CeO_2 core@shell samples. First, from Co_3O_4@CeO_2-4-250 to Co_3O_4@CeO_2-3-250 and then to Co_3O_4@CeO_2-1-250, the catalytic activity was enhanced with increasing Ce content. However, the catalytic activity decreased in the case of Co_3O_4@CeO_2-2-250 while further increasing the Ce content. This suggests that the catalytic activity values of our Co_3O_4@CeO_2 samples are highly dependent on Ce molar content, and tuning the component ratio of this kind of hetero-catalyst should constitute an efficient means for optimizing catalytic performance.

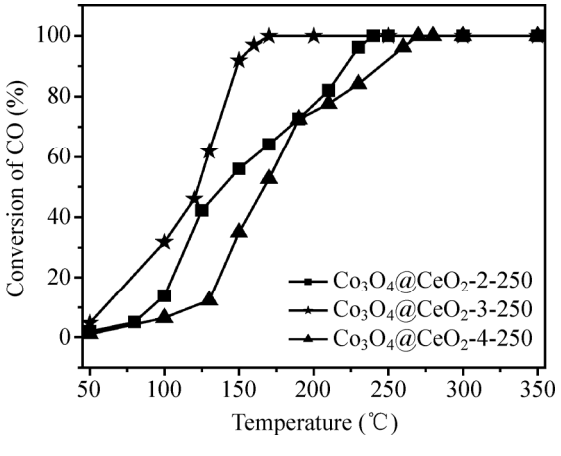

Figure 12 CO conversion curves of Co_3O_4@CeO_2-2-250, Co_3O_4@CeO_2-3-250, and Co_3O_4@CeO_2-4-250.

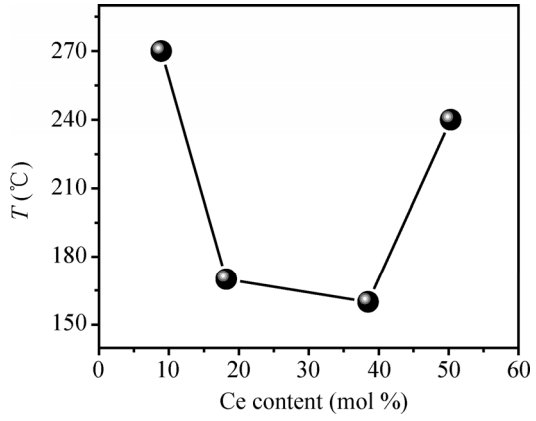

Figure 13 The relationship of Ce molar contents and the catalytic activity of the Co_3O_4@CeO_2 samples.

In our previous work, Co_3O_4@CeO_2 core@shell cubes were prepared by a similar self-assembly process. However, the utilization of Co^{2+} was as low as about 10%, which limits practical applicability. Here, the utilization of Co^{2+} in the preparation process of Co_3O_4@CeO_2 core@shell nanowires has been increased to about 80%. About 2 g of $Co(CO_3)_{0.5}(OH)\cdot 0.11H_2O$ nanowires were synthesized using a 500 mL Teflon-lined stainless steel autoclave. Then, more than 3 g of $Co(CO_3)_{0.5}(OH)\cdot 0.11H_2O$@$CeO_2$-1 was obtained by the self-assembly process using a 1 L flask. After calcination, more than 2.5 g of Co_3O_4@CeO_2-1-250 were obtained. In Fig. S16 in the ESM, it can be clearly seen that the above-mentioned mass-produced $Co(CO_3)_{0.5}(OH)\cdot 0.11H_2O$ and Co_3O_4@CeO_2-1-250 show no change in their wire-like structures. Meanwhile, Co_3O_4@CeO_2-1-250 obtained by mass production can also catalyze 100% CO conversion at the same temperature (see Fig. S17), which is more active than the previously reported Co_3O_4 nanowires, CeO_2 nanorods, CeO_2@Cu_2O nanocomposites, CeO_2-ZnO composite hollow microspheres, Ce-Mn binary oxide nanotubes, Co_3O_4@CeO_2 cubes, and $ZnCo_2O_4$@CeO_2 spheres because of the lower conversion temperature or the lower weight of effective catalysts (see Table 1 and Table S2 in the ESM) [32, 34–40]. Hence, it is likely that our Co_3O_4@CeO_2 core@shell nanowires, with excellent catalytic activity and stability for CO oxidation, may have considerable potential for practical applications such as automobile-exhaust gas-treatment catalysis.

Table 1 Characteristics of the as-obtained samples and their catalytic performance for CO oxidation

Sample	T (°C)[a]	Size (nm)[b]	T_{100} (°C)
Co_3O_4@CeO_2-1-250	250	5.9	160
Co_3O_4@CeO_2-1-350	350	10.1	250
Co_3O_4@CeO_2-1-500	500	12.7	>380
Co_3O_4 nanowires	250	9.9	360
Co_3O_4–CeO_2 mixtures	250	10.0	310
Co_3O_4–CeO_2 hybrids	250	10.1	300
Pure CeO_2 NPs	250	-	>350
Co_3O_4@CeO_2-2-250	250	5.9	240
Co_3O_4@CeO_2-3-250	250	5.9	170
Co_3O_4@CeO_2-4-250	250	5.9	270

[a] Calcination temperature

[b] Average size of Co_3O_4 NPs calculated from XRD patterns

4 Conclusions

In summary, we have successfully realized the facile, clean mass production of Co_3O_4@CeO_2 core@shell nanowires as catalysts for CO oxidation. The catalytic performance of the samples has been investigated systematically. Control experiments suggest that CO oxidation is likely to take place at the interface between Co_3O_4 and CeO_2 components. The high catalytic activity and stability of Co_3O_4@CeO_2 core@shell nanowires may be caused by the optimal synergistic effects of Co_3O_4 and CeO_2 components resulting from the specific core@shell structure. This also suggests that the catalytic activity of the Co_3O_4@CeO_2 core@shell nanowires strongly depends on the calcination temperatures and the component ratio between Co_3O_4 and CeO_2. Co_3O_4@CeO_2-1-250 obtained by calcination at 250 °C for 3 h with a Ce molar content of about 38.5% shows the best catalytic activity, reaching 100% CO conversion at temperatures as low as 160 °C. We believe that our Co_3O_4@CeO_2 core@shell nanowires may constitute promising candidates for CO oxidation in automobile-exhaust gas-treatment catalysts. This work details a feasible means for the fabrication of core@shell structures for the development and optimization of such hetero-nanocatalysts.

Acknowledgements

This work was supported by the financial aid from the National Natural Science Foundation of China (Nos. 91122030, 51272249, 21210001, 21221061 and 21401186), and the National Key Basic Research Program of China (No. 2014CB643802).

Electronic Supplementary Material: Supplementary material is available in the online version of this article at http://dx.doi.org/10.1007/s12274-015-0704-3.

References

[1] Hu, L. H.; Sun, K. Q.; Peng, Q.; Xu, B. Q.; Li, Y. D. Surface active sites on Co_3O_4 nanobelt and nanocube model catalysts for CO oxidation. *Nano Res.* **2010**, *3*, 363–368.

[2] Xie, X. W.; Li, Y.; Liu, Z. Q.; Haruta, M.; Shen, W. J. Low-temperature oxidation of CO catalysed by Co_3O_4 nanorods. *Nature* **2009**, *458*, 746–749.

[3] Song, W. Q.; Poyraz, A. S.; Meng, Y. T.; Ren, Z.; Chen, S. Y.; Suib, S. L. Mesoporous Co_3O_4 with controlled porosity: Inverse micelle synthesis and high-performance catalytic CO oxidation at −60 ˚C. *Chem. Mater.* **2014**, *26*, 4629−4639.

[4] Pandey, A. D.; Jia, C. J.; Schmidt, W.; Leoni, M.; Schwickardi, M.; Schüth, F.; Weidenthaler, C. Size-controlled synthesis and microstructure investigation of Co_3O_4 nanoparticles for low-temperature CO oxidation. *J. Phys. Chem. C* **2012**, *116*, 19405−19412.

[5] Jia, C. J.; Schwickardi, M.; Weidenthaler, C.; Schmidt, W.; Korhonen, S.; Weckhuysen, B. M.; Schüth, F. Co_3O_4-SiO_2 nanocomposite: A very active catalyst for CO oxidation with unusual catalytic behavior. *J. Am. Chem. Soc.* **2011**, *133*, 11279–11288.

[6] Lu, Z. H.; Jiang, H. L.; Yadav, M.; Aranishi, K.; Xu, Q. Synergistic catalysis of Au-Co@SiO_2 nanospheres in hydrolytic dehydrogenation of ammonia borane for chemical hydrogen storage. *J. Mater. Chem.* **2012**, *22*, 5065–5071.

[7] Arnal, P. M.; Comotti, M.; Schüth, F. High-temperature-stable catalysts by hollow sphere encapsulation. *Angew. Chem. Int. Ed.* **2006**, *45*, 8224–8227.

[8] Ge, J. P.; Zhang, Q.; Zhang, T. R.; Yin, Y. D. Core-satellite nanocomposite catalysts protected by a porous silica shell: Controllable reactivity, high stability, and magnetic recyclability. *Angew. Chem. Int. Ed.* **2008**, *47*, 8924–8928.

[9] Zhang, T. T.; Zhao, H. Y.; He, S. N.; Liu, K.; Liu, H. Y.; Yin, Y. D.; Gao, C. B. Unconventional route to encapsulated ultrasmall gold nanoparticles for high-temperature catalysis. *Acs. Nano* **2014**, *8*, 7297–7304.

[10] Yu, K.; Wu, Z. C.; Zhao, Q. R.; Li, B. X.; Xie, Y. High-temperature-stable Au@SnO_2 core/shell supported catalyst for CO oxidation. *J. Phys. Chem. C* **2008**, *112*, 2244–2247.

[11] Zhou, H. P.; Wu, H. S.; Shen, J.; Yin, A. X.; Sun, L. D.; Yan, C. H. Thermally stable Pt/CeO_2 hetero-nanocomposites with high catalytic activity. *J. Am. Chem. Soc.* **2010**, *132*, 4998–4999.

[12] Zhang, J.; Li, L. P.; Huang, X. S.; Li, G. S. Fabrication of Ag–CeO_2 core–shell nanospheres with enhanced catalytic performance due to strengthening of the interfacial interactions. *J. Mater. Chem.* **2012**, *22*, 10480–10487.

[13] Lee, I.; Zhang, Q.; Ge, J. P.; Yin, Y. D.; Zaera, F. Encapsulation of supported Pt nanoparticles with mesoporous silica for increased catalyst stability. *Nano Res.* **2011**, *4*, 115–123.

[14] Chen, J. C.; Zhang, R. Y.; Han, L.; Tu, B.; Zhao, D. Y. One-pot synthesis of thermally stable gold@mesoporous silica core–shell nanospheres with catalytic activity. *Nano Res.* **2013**, *6*, 871–879.

[15] Zhang, N.; Xu, Y. J. Aggregation- and leaching-resistant, reusable, and multifunctional Pd@CeO_2 as a robust nanocatalyst achieved by a hollow core–shell strategy. *Chem. Mater.* **2013**, *25*, 1979–1988.

[16] Lin, F.; Hoang, D. T.; Tsung, C. K.; Huang, W. Y.; Lo, S. H. Y.; Wood, J. B.; Wang, H.; Tang, J. Y.; Yang, P. D. Catalytic properties of Pt cluster-decorated CeO_2 nanostructures. *Nano Res.* **2011**, *4*, 61–71.

[17] Zhang, Y.; Hou, F.; Tan, Y. W. CeO_2 nanoplates with a hexagonal structure and their catalytic applications in highly selective hydrogenation of substituted nitroaromatics. *Chem. Commun.* **2012**, *48*, 2391–2393.

[18] Lee, Y. J.; He, G. H.; Akey, A. J.; Si, R.; Flytzani-Stephanopoulos, M.; Herman, I. P. Raman analysis of mode softening in nanoparticle $CeO_{2-\delta}$ and Au-$CeO_{2-\delta}$ during CO oxidation. *J. Am. Chem. Soc.* **2011**, *133*, 12952–12955.

[19] Xu, L. S; Ma, Y. S.; Zhang, Y. L.; Jiang, Z. Q.; Huang, W. X. Direct evidence for the interfacial oxidation of CO with hydroxyls catalyzed by Pt/oxide nanocatalysts. *J. Am. Chem. Soc.* **2009**, *131*, 16366–16367.

[20] Tian, J.; Sang, Y. H.; Zhao, Z. H.; Zhou, W. J.; Wang, D. Z.; Kang, X. L.; Liu, H.; Wang, J. Y.; Chen, S. W.; Cai, H. Q.; et al. Enhanced photocatalytic performances of CeO_2/TiO_2 nanobelt heterostructures. *Small* **2013**, *9*, 3864–3872.

[21] Mak, A. C.; Yu, C. L.; Yu, J. C.; Zhang, Z. D.; Ho, C. A lamellar ceria structure with encapsulated platinum nanoparticles. *Nano Res.* **2008**, *1*, 474–482.

[22] Wang, X.; Liu, D. P.; Song, S. Y.; Zhang, H. J. Pt@CeO_2 multicore@shell self-assembled nanospheres: Clean synthesis, structure optimization, and catalytic applications. *J. Am. Chem. Soc.* **2013**, *135*, 15864−15872.

[23] Kayama, T.; Yamazaki, K.; Shinjoh, H. Nanostructured ceria-silver synthesized in a one-pot redox reaction catalyzes carbon oxidation. *J. Am. Chem. Soc.* **2010**, *132*, 13154–13155.

[24] Guo, H.; He, Y. B.; Wang, Y. P.; Liu, L. X.; Yang, X. J.; Wang, S. X.; Huang, Z. J.; Wei, Q. Y. Morphology-controlled synthesis of cage-bell Pd@CeO_2 structured nanoparticle aggregates as catalysts for the low-temperature oxidation of CO. *J. Mater. Chem. A* **2013**, *1*, 7494–7499.

[25] Li, B. X.; Gu, T.; Ming, T.; Wang, J. X.; Wang, P.; Wang, J. F.; Yu, J. C. (Gold core)@(ceria shell) nanostructures for plasmon-enhanced catalytic reactions under visible light. *ACS Nano* **2014**, *8*, 8152–8162.

[26] Wu, B. H.; Zhang, H.; Chen, C.; Lin, S. C.; Zheng, N. F. Interfacial activation of catalytically inert Au (6.7 nm)–Fe_3O_4 dumbbell nanoparticles for CO oxidation. *Nano Res.* **2009**, *2*, 975–983.

[27] Wang, B.; Zhu, T.; Wu, H. B.; Xu, R.; Chen, J. S.; Lou, X. W. Porous Co_3O_4 nanowires derived from long $Co(CO_3)_{0.5}(OH)\cdot 0.11H_2O$ nanowires with improved supercapacitive properties. *Nanoscale* **2012**, *4*, 2145–2149.

[28] Zhen, J. M.; Wang, X.; Liu, D. P.; Song, S. Y.; Wang, Z.; Wang, Y. H.; Li, J. Q.; Wang, F.; Zhang, H. J. Co_3O_4@CeO_2 core@shell cubes: Designed synthesis and optimization of catalytic properties. *Chem. Eur. J.* **2014**, *20*, 4469–4473.

[29] Luo, J. Y.; Meng, M.; Zha, Y. Q.; Guo, L. H. Identification of the active sites for CO and C_3H_8 total oxidation over nanostructured CuO−CeO_2 and Co_3O_4−CeO_2 catalysts. *J. Phys. Chem. C* **2008**, *112*, 8694–8701.

[30] Hornés, A.; Hungría, A. B.; Bera, P.; Cámara, A. L.; Fernández-García, M.; Martínez-Arias, A.; Barrio, L.; Estrella, M.; Zhou, G.; Fonseca, J. J.; et al. Inverse CeO_2/CuO catalyst as an alternative to classical direct configurations for preferential oxidation of CO in hydrogen-rich stream. *J. Am. Chem. Soc.* **2010**, *132*, 34−35.

[31] Wu, H.; Xu, M.; Wang, Y. C.; Zheng, G. F. Branched Co_3O_4/Fe_2O_3 nanowires as high capacity lithium-ion battery anodes. *Nano Res.* **2013**, *6*, 167–173.

[32] Li, W. Y.; Xu, K. B.; An, L.; Jiang, F. R.; Zhou, X. Y.; Yang, J. M.; Chen, Z. G.; Zou, R. J.; Hu, J. Q. Effect of temperature on the performance of ultrafine MnO_2 nanobelt supercapacitors. *J. Mater. Chem. A* **2014**, *2*, 1443–1447.

[33] Wang, F.; Wang, X.; Liu, D. P.; Zhen, J. M.; Li, J. Q.; Wang, Y. H.; Zhang, H. J. High-performance $ZnCo_2O_4$@CeO_2 core@shell microspheres for catalytic CO oxidation. *ACS Appl. Mater. Interfaces* **2014**, *6*, 22216–22223.

[34] Tüysüz, H.; Hwang, Y. J.; Khan, S. B.; Asiri, A. M.; Yang, P. D. Mesoporous Co_3O_4 as an electrocatalyst for water oxidation. *Nano Res.* **2013**, *6*, 47–54.

[35] Sun, Y.; Lv, P.; Yang, J. Y.; He, L.; Nie, J. C.; Liu, X. W.; Li, Y. D. Ultrathin Co_3O_4 nanowires with high catalytic oxidation of CO. *Chem. Commun.* **2011**, *47*, 11279–11281.

[36] Li, J.; Zhang, Z. Y.; Tian, Z. M.; Zhou, X. M.; Zheng, Z. P.; Ma, Y. Y.; Qu, Y. Q. Low pressure induced porous nanorods of ceria with high reducibility and large oxygen storage capacity: synthesis and catalytic applications. *J. Mater. Chem. A* **2014**, *2*, 16459–16466.

[37] Bao, H. Z.; Zhang, Z. H.; Hua, Q.; Huang, W. X. Compositions, structures, and catalytic activities of CeO_2@Cu_2O nanocomposites prepared by the template-assisted method. *Langmuir* **2014**, *30*, 6427−6436.

[38] Xie, Q. S.; Zhao, Y.; Guo, H. Z.; Lu, A. L.; Zhang, X. X.; Wang, L. S.; Chen, M. S.; Peng, D. L. Facile preparation of well-dispersed CeO_2–ZnO composite hollow microspheres with enhanced catalytic activity for CO oxidation. *ACS Appl. Mater. Interfaces* **2014**, *6*, 421–428.

[39] Chen, G. Z.; Rosei, F.; Ma, D. L. Interfacial reaction-directed synthesis of Ce–Mn binary oxide nanotubes and their applications in CO oxidation and water treatment. *Adv. Funct. Mater.* **2012**, *22*, 3914–3920.

[40] Guan, Y. J.; Hensen, E. J. M.; Liu, Y.; Zhang, H. D.; Feng, Z. C.; Li, C. Template-free synthesis of sphere, rod and prism morphologies of CeO_2 oxidation catalysts. *Catal. Lett.* **2010**, *137*, 28–34.